

DTP/92/88
UCD-92-29
LU-TP-92-33
December 1992

Properties of Soft Radiation Near $t\bar{t}$ and W^+W^- Threshold

Yu.L. Dokshitzer

*Department of Theoretical Physics, University of Lund
Sölvegatan 14A, S-22362 Lund, Sweden*

V.A. Khoze

*Department of Physics, University of Durham
Durham DH1 3LE, England*

Lynne H. Orr

*Department of Physics, University of California
Davis, CA 95616, USA.*

and

W.J. Stirling

*Departments of Physics and Mathematical Sciences, University of Durham
Durham DH1 3LE, England*

Abstract

We discuss the characteristic interference features of soft radiation in the threshold production of heavy unstable particles: soft gluon radiation in $e^+e^- \rightarrow t\bar{t}$ and soft photon radiation in $e^+e^- \rightarrow W^+W^-$. We show that the heavy particle decay width controls the interference between the emission off the final state particles. As a result, the radiation pattern may provide a way of measuring the decay width of the heavy particles.

1 Introduction

Heavy unstable charged particles can emit radiation both before and after they decay. The analysis of such radiation is a complex issue, depending sensitively on the timescale of the emission compared to the lifetime of the unstable particle [1]. In particular, the radiation pattern can be very different according to whether the radiation occurs predominantly during the production stage or after the particle has decayed [2].

There are several important examples of such effects which are directly relevant to present and future high-energy colliders. As a specific example, consider the production and decay of a $t\bar{t}$ pair in high-energy e^+e^- annihilation. With a mass of at least 91 GeV [3], the top quark can decay to a real W boson and a b quark. The width Γ_t for this decay is quite large — so large that the top weak lifetime can be as short as strong interaction timescales. The resulting interplay between the strong and weak interactions of the top quark gives rise to interesting physical effects. For example, if top is heavier than ~ 100 GeV, then Γ_t can be greater than the typical hadronic scale $\mu \sim 1 \text{ fm}^{-1}$ and it may decay *before* it has time to hadronize [4-6]. In particular, $t\bar{t}$ resonances may never be formed. Here we are interested in the perturbative aspects of the strong-weak interplay: decay versus gluon bremsstrahlung. Reference [2] discussed soft gluon radiation in $e^+e^- \rightarrow t\bar{t}$ and showed that gluons radiated in top production and decay can interfere, and how much they do depends on the top width. This means that top production and decay should not be treated separately — the gluon distribution in top events is not what one might naively guess. Furthermore, this width effect might be useful; the sensitivity of the soft gluon distribution to Γ_t suggests a way to measure it [2,7]. The width dependence of the gluon distribution at high collision energies was studied in Ref. [2]; however, it was found that the configurations with the most sensitivity to Γ_t were also the least likely to occur.

In this paper we consider on soft gluon radiation near the $t\bar{t}$ threshold. The top quarks are produced nearly at rest and essentially do not radiate. The width dependence is a result of interference between gluons radiated in the two decays, which does not play an important role at higher energies. Near the production threshold, the amount of interference between gluons from the b and \bar{b} is controlled by the top width, and what matters is the size of Γ_t relative to the gluon energy. Thus we will see that when the top width and the gluon energy are more or less the same order of magnitude, the radiation pattern is sensitive to Γ_t .

A second process which exhibits similar features is the emission of photon radiation in the process $e^+e^- \rightarrow W^+W^- \rightarrow f\bar{f}'f\bar{f}'$. The radiation pattern of a soft photon of energy ω is sensitive to the W decay width for $\omega \sim \Gamma_W$. Here there is the additional complication of radiation off the initial state as well, but, as we shall see, this can easily be taken into account.

In principle, therefore, the study of the soft gluonic and photonic radiation in $t\bar{t}$ and W^+W^- production provides a basis for determining the decay width of the heavy

particle. In practice, however, there are many difficulties. The measurement of the radiation pattern in top quark production requires the separation and identification of a soft gluon jet (typically with energy $\omega \sim 5$ GeV). In the case of photons radiated in W^+W^- production, while identification of relatively soft photons might not pose too many problems, the event rates are low for the anticipated luminosities of future e^+e^- colliders. Nevertheless, we believe these issues are worth exploring for several reasons. First, on a theoretical level there are several features of the radiation patterns that show interesting interference effects which are at first sight counter-intuitive. Second, the ‘traditional’ methods of measuring the masses and decay widths by threshold scanning are not without their own problems. Especially for $t\bar{t}$ production at high-energy e^+e^- linear colliders, the structure of the threshold is smeared by beam-induced effects, intrinsic energy spread etc. On the theoretical level, the measurement of Γ_t from the shape of the cross section as a function of beam energy near threshold is a delicate issue. For $e^+e^- \rightarrow W^+W^-$, the threshold scan strategy requires a detailed calculation of higher order electroweak effects including width effects and initial state radiation. To our knowledge, a comprehensive one-loop calculation including the width effects has not yet been completed. An attempt to incorporate Γ_W into the tree-level formulae has been made in Ref. [8] (see also Ref. [9]). These results however are seriously affected by initial state radiation and other effects like the final-state Coulomb attraction near the W^+W^- threshold [10, 11]. As a general comment, one might argue that the W width is already known to fairly high precision ($\Gamma_W = 2.15 \pm 0.11$ GeV [12]) from *indirect* measurements using W production cross sections in $p\bar{p}$ colliders. Nevertheless, we believe it is important to obtain a *direct* measurement of this important Standard Model parameter as well.

In this paper, therefore, we will focus mainly on the theoretical features of soft radiation in $t\bar{t}$ and W^+W^- production. Some illustrative numerical results for $t\bar{t}$ production are presented; a more complete numerical treatment of the W^+W^- case, particularly with reference to LEP200, is deferred to another paper [13]. We believe that our conclusions will show that a more detailed experimental study (event rates, detector capabilities, etc.) is certainly warranted. The remainder of the paper is organized as follows. In Sections 2 and 3 we discuss the radiation pattern, for gluons in $t\bar{t}$ production and photons in W^+W^- production respectively, near threshold in detail. In Section 4 we present numerical results for top production and discuss prospects for measuring Γ_t . We conclude in Section 5. Appendices contain a semi-classical derivation of the radiation pattern and further details of the calculation of the distributions.

2 Soft radiation pattern

We are interested in emission of a gluon in the process $e^+e^- \rightarrow t\bar{t} \rightarrow WWb\bar{b}$ and of a photon in the process $e^+e^- \rightarrow W^+W^- \rightarrow f\bar{f}'f\bar{f}'$. Although the analysis of the final

state radiation in both processes is very similar, the latter process is complicated by the additional contributions from initial state radiation. To begin with, therefore, we discuss the $t\bar{t}$ case, and extend the analysis to W^+W^- production in the next Section.

The general result for soft gluon radiation in $e^+e^- \rightarrow t\bar{t} \rightarrow WWb\bar{b}$ was presented in reference [2] (see also [7]). Here we focus on the particular case of radiation close to the $t\bar{t}$ threshold. There are two advantages in this. First, the production cross section is largest just above threshold. Second, near threshold the top quarks are almost at rest and only the b and \bar{b} radiate. While it is not obvious that the top quark width should enter at all if only the b -quarks radiate, we can understand its role as follows. Consider two cases of gluon radiation from a $b\bar{b}$ pair. If the quarks could radiate independently, with no interference, the gluon distribution would be proportional to

$$\mathcal{R}_{\text{indep.}} = \mathcal{R}_1 + \mathcal{R}_2 = \frac{v_1^2 \sin^2 \theta_1}{(1 - v_1 \cos \theta_1)^2} + \frac{v_2^2 \sin^2 \theta_2}{(1 - v_2 \cos \theta_2)^2}, \quad (2.1)$$

where v_i is the velocity of the b (\bar{b}), and θ_i is the angle between the b (\bar{b}) and the gluon for $i = 1$ (2). (Note that in what follows we will make a distinction between v_1 and v_2 although in practice, for the case of $e^+e^- \rightarrow t\bar{t} \rightarrow W^+W^-b\bar{b}$ in the centre-of-mass frame, we always have $v_1 = v_2$.) In the other extreme, with interference we have coherent emission, and the gluon distribution looks like

$$\begin{aligned} \mathcal{R}_{\text{coher.}} &= \mathcal{R}_{\text{indep.}} + 2\mathcal{J}, \\ \mathcal{J} &\equiv \frac{v_1 v_2 (\cos \theta_1 \cos \theta_2 - \cos \theta_{12})}{(1 - v_1 \cos \theta_1)(1 - v_2 \cos \theta_2)}, \end{aligned} \quad (2.2)$$

where θ_{12} is the angle between the b and the \bar{b} . This is just the familiar antenna pattern for emission from a quark-antiquark pair; the interference is $2\mathcal{J}$. Note that these patterns can be quite different and the interference can be constructive or destructive. In particular, and as we shall discuss in more detail later (and see Appendix E), coherent emission exhibits angular ordering behavior, *i.e.* if we integrate over the azimuthal angle about the direction of quark 1, all radiation from quark 1 is suppressed for angles θ_1 such that [14,15]

$$v_2 \cos \theta_{12} < \cos \theta_1 < \cos \theta_c \simeq v_1. \quad (2.3)$$

The factor v_1 on the right-hand-side takes account of the screening effects due to the mass of quark 1 (dead-cone).

Now recall that in the case of interest the b and \bar{b} are produced by the decays of the t and \bar{t} . If the top lifetime is very short compared to the characteristic time for emitting a gluon of energy ω (*i.e.* $\Gamma_t \gg \omega$), the b and \bar{b} are produced nearly instantaneously, and we expect coherent gluon emission, with the gluon distribution determined by $\mathcal{R}_{\text{coher.}}$. If however the top lifetime is very long (*i.e.* $\Gamma_t \ll \omega$), the b and

\bar{b} are produced at very different times and thus will radiate independently; the gluon distribution is then given by $\mathcal{R}_{\text{indep.}}$. The ratio Γ_t/ω of the top width to the gluon energy controls the amount of interference. The full distribution we show below was derived from standard Feynman diagram techniques in Ref. [2]. But in fact it can be derived from simple semi-classical wave arguments – see Appendix A.

Following reference [2], the radiation pattern can be presented as a probability density, normalized to the lowest order cross section:

$$dN \equiv 1/\sigma_0 d\sigma_g = \frac{d\omega}{\omega} \frac{d\Omega}{4\pi} \frac{C_F \alpha_s}{\pi} \mathcal{N}. \quad (2.4)$$

where $C_F = 4/3$ is the QCD colour factor. Near threshold, we have

$$\begin{aligned} \mathcal{N} &\equiv (1 - \chi(\omega)) \cdot \mathcal{R}_{\text{indep.}} + \chi(\omega) \cdot \mathcal{R}_{\text{coher.}} \\ &= \mathcal{R}_{\text{indep.}} + 2\chi(\omega) \cdot \mathcal{J}, \end{aligned} \quad (2.5)$$

where $\mathcal{R}_{\text{indep.}}$ and $\mathcal{R}_{\text{coher.}}$ are given in eqns.2.1 and 2.2 (with $v_1 = v_2 = v_b$) and we have introduced the profile function

$$\chi(\omega) = \frac{\Gamma^2}{\Gamma^2 + \omega^2}, \quad (2.6)$$

The factor χ , which depends on the decay width and gluon energy, determines the amount of interference, and as stated above we have in the limits of large and small width,

$$\mathcal{N} = \mathcal{R}_{\text{indep.}} \quad \text{for } \omega \gg \Gamma, \quad (2.7a)$$

$$\mathcal{N} = \mathcal{R}_{\text{coher.}} \quad \text{for } \omega \ll \Gamma. \quad (2.7b)$$

Evidently, we have maximal sensitivity to Γ_t for $\omega \sim \Gamma_t$, and this provides a possible basis for measuring the width. For gluon emission we must in addition impose $\omega > \mu \sim 1 \text{ fm}^{-1}$, in order to remain in the perturbative regime.

Before performing a detailed numerical study of the above to investigate the actual sensitivity to Γ_t in different angular configurations, we make some additional comments.

- (i) The numerator of the \mathcal{J} term in (2.2) can be written as

$$\cos \theta_1 \cos \theta_2 - \cos \theta_{12} = -\sin \theta_1 \sin \theta_2 \cos \phi_{12} \quad (2.8)$$

with ϕ_{12} the relative azimuth between \vec{p}_1 and \vec{p}_2 with respect to the gluon direction, \vec{k} . Thus an immediate consequence of the interference is that the azimuthal symmetry of the radiation about the b -quark directions is destroyed. Note also that the expression (2.8) vanishes when the direction of the gluon momentum is chosen to be close to that of one of the quarks, $\theta_1 \ll \theta_{12}$ or $\theta_2 \ll \theta_{12}$. Therefore the ω -dependence of the radiation pattern (2.5) can reveal itself only if the gluon emission angles are not small compared to the opening angle of the b and \bar{b} .

- (ii) It is fairly straightforward to integrate over the angle of the emitted gluon and obtain the *total* probability for the radiation of a gluon of given energy. (In a sense this is a formal procedure, since in practice the gluon jet will only be identified when separated from other final state jets and from the beam.) Full details are given in Appendix B – here we present only the result:

$$\frac{dN}{d\omega} = \frac{C_F\alpha_s}{\pi\omega} \left\{ (1 - \chi(\omega)) \left[\frac{1}{v_1} \log \frac{1+v_1}{1-v_1} + \frac{1}{v_2} \log \frac{1+v_2}{1-v_2} - 4 \right] + \chi \left[\frac{1}{r} \log \frac{1+r}{1-r} - 2 \right] \right\}. \quad (2.9)$$

where

$$r = \frac{\sqrt{\psi^2 - 1}}{\psi}$$

$$\psi = \frac{p_1 \cdot p_2}{M_1 M_2} = \frac{(1 - v_1 v_2 \cos \theta_{12})}{\sqrt{(1 - v_1^2)(1 - v_2^2)}}. \quad (2.10)$$

Note the logarithmic collinear singularities which dominate the integrated distribution in the ultra-relativistic limit $v_i \rightarrow 1$. In fact for $(1 - v_i) \ll 1$ and for θ_{12} values not particularly close to 0, we have (Appendix B)

$$\frac{dN}{d\omega} \approx \frac{C_F\alpha_s}{\pi\omega} \left\{ \ln \frac{2}{1-v_1} + \ln \frac{2}{1-v_2} - 4 + 2\chi(\omega) \left[\ln \frac{1 - \cos \theta_{12}}{2} + 1 \right] \right\}. \quad (2.11)$$

Note that the second ω -dependent term in (2.11) *enhances* or *depletes* the radiation according to whether θ_{12} is larger or smaller than $\Theta_{\text{crit}} \approx 75^\circ$ (Appendix B).

3 Soft photon radiation in $e^+e^- \rightarrow W^+W^-$

Before presenting our numerical results for the $t\bar{t}$ case we discuss in this section the extension of the above analysis to soft photon radiation near threshold in the process $e^+e^- \rightarrow W^+W^- \rightarrow f\bar{f}'f\bar{f}'$. Once again the radiation pattern includes contributions from the WW production and decay antennae, together with interferences between them. As was demonstrated in Ref. [16], the radiation at the production stage (the $\widehat{W\bar{W}}$ antenna) is given by the classical current expression, as for the $\widehat{t\bar{t}}$ antenna [2], irrespective of the choice of gauge. Apart from overall couplings, colour factors and charges, there are only two main differences. First, there are additional contributions from initial state radiation. These pose no particular problems in practice as long as the final state particles, including the photon, are kept well away from the beam direction. As shown in reference [17], when all the final state particles are exactly

transverse to the beam direction, the initial state radiation simply adds a small, constant “background term” to the radiation pattern, which is of course independent of the decay width of the decaying W 's. We note also that near the WW threshold there are kinematic constraints which are different for initial and final state radiation. The former is limited by the maximal kinematically allowed energy

$$\omega < \omega_{max}^{IS} = M_W v_W^2 \ll M_W, \quad (3.12)$$

whereas the constraint on the energy emitted in the course of decay is much less severe,

$$\omega < \omega_{max}^{FS} = \frac{M_W^2 - m_0^2}{2M_W} \sim M_W, \quad (3.13)$$

where m_0 is the minimal invariant mass of the W decay products.

Since we are mainly interested in the region of photon energies $\omega \sim \Gamma$ where the width has an important effect on the radiation pattern, we can imagine choosing a kinematic region,

$$\omega \sim \Gamma \ll M_W v_W^2 \ll M_W, \quad (3.14)$$

where the soft bremsstrahlung approximation can be used for both initial and final state radiation, without having to worry about the kinematic restrictions on the photon energy. A derivation of the radiation pattern for this situation using the classical picture considered in Appendix A is presented in Appendix C.

A second difference arises when we consider extending the analysis to *hadronic* W decays, *i.e.* to $W \rightarrow q\bar{q}'$. This is of course the dominant W decay channel – about 44% of WW pairs decay to a four-jet final state, and only about 5% of the decays have purely leptonic (e or μ) final states. In order to achieve a measureable event rate, therefore, it will probably be necessary to demand at least one hadronically decaying W .

For $W \rightarrow q\bar{q}'$ both decay products can now radiate, and the pattern of radiation is correspondingly more complicated. Thus the electromagnetic current caused by the leptonic decay $W^+(q) \rightarrow e^+(p)\nu_e(\bar{p})$,

$$j_\ell^\mu = \frac{p^\mu}{(kp)} - \frac{q^\mu}{(kq)}, \quad (3.15)$$

becomes, for the hadronic decay, $W^+(q) \rightarrow u(p)\bar{d}(\bar{p})$,

$$j_h^\mu = Q \frac{p^\mu}{(kp)} + (1-Q) \frac{\bar{p}^\mu}{(k\bar{p})} - \frac{q^\mu}{(kq)}, \quad (3.16)$$

where $Q = 2/3$ is the electric charge of the u quark. The general final state radiation pattern can then be formed from these currents in the usual way,

$$\mathcal{N} \propto (j_1^\mu e_\mu)^2 + (j_2^\mu e_\mu)^2 - 2\chi(\omega) \cdot (j_1^\mu e_\mu)(j_2^\mu e_\mu) \quad (3.17a)$$

$$= (1 - \chi(\omega)) \cdot [(j_1^\mu e_\mu)^2 + (j_2^\mu e_\mu)^2] + \chi(\omega) \cdot [(j_1^\mu - j_2^\mu) e_\mu]^2. \quad (3.17b)$$

Equivalent formulae to those considered above for gluon radiation in t decay can then be derived. The analysis is simplest if we assume that in each W decay the quark and the accompanying antiquark are *anti-parallel*, otherwise additional angles have to be introduced; this is certainly justified if the W 's are produced at rest. If we make the further assumption that the velocities of the quark and antiquark in the decay are equal, and that experimentally quark and antiquark jets cannot be distinguished, then we obtain the radiation patterns for the two-quark and the one-quark-one-leptonic decays (see Appendix D):

$$\begin{aligned} \mathcal{N}^{(qq)} &= \mathcal{R}_1 \left[\frac{(2Q-1)^2 + v_1^2 \cos^2 \theta_1}{(1 + v_1 \cos \theta_1)^2} \right] + \mathcal{R}_2 \left[\frac{(2Q'-1)^2 + v_2^2 \cos^2 \theta_2}{(1 + v_2 \cos \theta_2)^2} \right] \\ &+ 2 \chi(\omega) \cdot \mathcal{J} \left[\frac{v_1 v_2 \cos \theta_1 \cos \theta_2}{(1 + v_1 \cos \theta_1)(1 + v_2 \cos \theta_2)} \right]; \end{aligned} \quad (3.18)$$

$$\begin{aligned} \mathcal{N}^{(q\ell)} &= \mathcal{R}_1 \left[\frac{(2Q-1)^2 + v_1^2 \cos^2 \theta_1}{(1 + v_1 \cos \theta_1)^2} \right] + \mathcal{R}_2 \\ &+ 2 \chi(\omega) \cdot \mathcal{J} \left[\frac{v_1 \cos \theta_1}{1 + v_1 \cos \theta_1} \right], \end{aligned} \quad (3.19)$$

where $Q = Q' = \frac{2}{3}$ and v_1, v_2 denote the velocities of the up-type quark and antiquark respectively for the $(q\bar{q})$ case, and the quantities $\mathcal{R}_1, \mathcal{R}_2$ and \mathcal{J} are defined in (2.1) and (2.2). These expressions are the analogues of the $t\bar{t}$ result (2.5) derived above. The differential cross section is obtained in the same way, with the substitution $C_F \alpha_s \rightarrow \alpha$.

To study the θ_{12} dependence of the *total* photon yield (again ignoring the isolation cuts which will be required in practice) one has to evaluate the integrals over the photon radiation angle of the interference terms in (3.18,3.19). These integrals are finite at $v_1 = v_2 = 1$ and so we can use the ultra-relativistic approximation in this case. As shown in Appendix D, the total photon yield takes the form

$$\omega \frac{dN^{(\alpha\beta)}}{d\omega} = \frac{\alpha}{\pi} \cdot B^{\alpha\beta} \cdot \mathcal{T}^{(\alpha\beta)} \left(\theta_{12}, \frac{\omega}{\Gamma} \right) \quad (3.20)$$

where we denote by $(\alpha\beta)$ decay channels of the W^+W^- system

$$\begin{aligned} (\alpha\beta) = (\ell\ell) &: W^+W^- \rightarrow \ell\nu + \ell\nu, \\ (q\ell) &: W^+W^- \rightarrow \ell\nu + q\bar{q}, \\ (qq) &: W^+W^- \rightarrow q\bar{q} + q\bar{q}. \end{aligned} \quad (3.21)$$

The branching ratios are approximately $B^{\ell\ell} = 4/81$, $B^{q\ell} = 24/81$ and $B^{qq} = 36/81$. for $\ell = e, \mu$. We have

$$\mathcal{T}^{(\ell\ell)} = \mathcal{R}_{\text{indep.}}^{(\ell)} + \mathcal{R}_{\text{indep.}}^{(\ell)} + 2\chi(\omega) \cdot \left[\ln \frac{1 - \cos \theta_{12}}{2} + 1 \right], \quad (3.22a)$$

$$\mathcal{T}^{(q\ell)} = \mathcal{R}_{\text{indep.}}^{(q)} + \mathcal{R}_{\text{indep.}}^{(\ell)} + 2\chi(\omega) \cdot \left[\ln \frac{\sin \theta_{12}}{2} + 1 \right], \quad (3.22b)$$

$$\mathcal{T}^{(qq)} = \mathcal{R}_{\text{indep.}}^{(q)} + \mathcal{R}_{\text{indep.}}^{(q)} + 2\chi(\omega) \cdot \left[\ln \frac{\sin \theta_{12}}{2} + 1 \right], \quad (3.22c)$$

with the θ_{12} -independent contributions

$$\mathcal{R}_{\text{indep.}}^{(\ell)} = \mathcal{I}(v) = \frac{1}{v} \ln \frac{1+v}{1-v} - 2 \approx \ln \frac{2}{1-v} - 2, \quad (3.23a)$$

$$\mathcal{R}_{\text{indep.}}^{(q)} = Q^2 \mathcal{I}(v) + (1-Q)^2 \mathcal{I}(\bar{v}) - 2Q(1-Q) + \mathcal{O}(1-v^2, 1-\bar{v}^2). \quad (3.23b)$$

In (3.23a), v is the velocity of a charged lepton; v and \bar{v} in (3.23b) are the velocities of the up -type quark (antiquark) and, respectively, $down$ -type antiquark (quark) originating from W^+ (W^-). Once again, the ω dependent terms in (3.22a) can be either positive (larger θ_{12}) or negative (smaller θ_{12}). For the double-leptonic channel the critical angle is the same as for the $t\bar{t}$ case ($\approx 75^\circ$) whereas with at least one hadronic decay channel it follows from (3.22b) and (3.22c) that the corresponding critical angle is approximately 47° .

Unfortunately, the pure “partonic” prediction (3.23b) for the independent photon radiation off the quark-antiquark antenna is too naive in practice, since quark velocities are not well-defined for light quarks, and the result takes no account of the hadronization process where integer charge hadrons are formed and indirect photons from hadron decays appear.

However these complications do not affect the main physical property of (3.22), namely the fact that the θ_{12} -dependent (and thus the Γ -dependent) part of the photon radiation pattern *is* under control. As long as W^+ and W^- initiated jets evolve independently from one another, the extra yield of indirect photons remains insensitive to the event geometry.

Finally, we note that an exactly analogous study could be performed for the soft photon radiation pattern in the process $e^+e^- \rightarrow Z^0 Z^0 \rightarrow f\bar{f}f'\bar{f}'$. The four charged particles in the final state give rise to a rich interference structure, as for the four-jet decays of the WW pair discussed above. The four charged leptonic decays of the $Z^0 Z^0$ pair would provide a particularly clean environment in which to study this, but in practice the event rates would be prohibitively low.

4 Numerical results for top

4.1 Preliminary remarks

In this Section we illustrate the behavior of soft radiation near threshold with some examples. We will discuss the gluon distributions in $t\bar{t}$ events case in some detail,

and show a single example for photons in the W^+W^- case. Our emphasis will be on the influence of the width Γ on the radiation pattern. As discussed above, one might expect that, because of the top quark's large width (and hence short lifetime), the $b\bar{b}$ pair would radiate coherently, as if they had been produced directly. We will see that the correct soft gluon distributions can differ considerably from those which arise from that expectation. We will explore the sensitivity of the radiation patterns to Γ and at the end we will consider briefly to what extent this sensitivity might be useful for measuring Γ .

Before presenting our numerical results it is helpful to summarize the results from Section 2 that are most relevant to what follows. Recall that the gluon emission probability density is given by Eq. (2.4) with

$$\mathcal{N} = \frac{v^2 \sin^2 \theta_1}{(1 - v \cos \theta_1)^2} + \frac{v^2 \sin^2 \theta_2}{(1 - v \cos \theta_2)^2} + 2\chi(\omega) \frac{v^2 (\cos \theta_1 \cos \theta_2 - \cos \theta_{12})}{(1 - v \cos \theta_1)(1 - v \cos \theta_2)}, \quad (4.24)$$

and $\chi(\omega) \equiv \frac{\Gamma^2}{\Gamma^2 + \omega^2}$; $0 \leq \chi \leq 1$. The profile function χ determines the amount of interference between radiation off the b and \bar{b} : for $\Gamma = 0$, we have $\chi = 0$ and the interference is suppressed, whereas for $\Gamma \gg \omega$, $\chi \rightarrow 1$ and we have the full coherent emission mentioned in the previous paragraph. Finally, note again that

- The only dependence on the relative geometry of the b and \bar{b} appears in the interference term; independent emission has no θ_{12} dependence.
- In contrast to the high energy case [2] where we saw mostly destructive interference, the interference term here can have either sign. We will see explicitly below that, as pointed out earlier, it tends to be constructive for small θ_{12} and destructive for large θ_{12} .
- From the form of χ it is clear that we have maximum sensitivity to the width when $\Gamma \sim \omega$ (χ not near 0 or 1), *i.e.*, when the energy of the radiation is comparable to the width.

The remainder of Section 4 amounts to an elaboration of these points.

Now, these interference width effects influence the radiation pattern, as illustrated in the differential distributions we present below. The behavior discussed above would be clearly evident if the differential distributions were observable, *i.e.* if we had access to arbitrary gluon energies and arbitrarily large numbers of events, and we could observe partons directly. Of course, in the real world there are jets and limited statistics. Therefore in what follows we make some concessions to reality by also considering integrated distributions. Furthermore we assume that the gluon will be 'detected' as a soft jet, and so we take 5 GeV as the minimum observable gluon energy. However, this is no substitute for realistic simulations, nor is it meant to be; our results are meant to suggest the kinds of distributions that would be interesting to study.

The results presented below are more or less independent of the top mass. If we treat Γ as a parameter, m_t comes into (4.24) only weakly through the b quark velocity v . For definiteness, we use $v = 0.9944$, which corresponds to $m_t = 140$ GeV for $m_b = 5$ GeV and $m_W = 80$ GeV. A further generalization is possible if ω is kept fixed: then Γ and ω only enter through χ . Now, what values of χ are relevant for accessible gluon energies and interesting top masses? For our canonical $m_t = 140$ GeV, $\Gamma \approx 0.7$ GeV in the Standard Model. Taking $\omega = 5$ GeV, we obtain $\chi = 0.02$, which is rather close to zero. The gluon distribution is therefore close to that for *independent* emission, not coherent emission as we might naively guess. The story is slightly different for larger m_t because the Standard Model width grows as m_t^3 . For example, for $m_t = 200$ GeV, Γ approaches 3 GeV and with $\omega = 5$ GeV we have $\chi \approx 0.3$. So the heavier the top quark, the larger are the relevant values of Γ and χ .

4.2 Soft gluon distributions

4.2.1 Radiation out of the $b\bar{b}$ plane

\mathcal{N} takes a particularly simple form for gluons radiated perpendicular to the plane of the $b\bar{b}$ pair. In this case, $\theta_1 = \theta_2 = \pi/2$ and

$$\mathcal{N} \propto 1 - \chi \cos \theta_{12}. \quad (4.25)$$

The width and energy dependence are given, via χ , by the extent of the deviation from constant behavior of the gluon emission probability as a function of θ_{12} . This is illustrated in Fig. 1, where we show¹ $\omega(dN/d\omega d\Omega)$ as a function of θ_{12} for $\chi = 0, \frac{1}{3}, \frac{2}{3}$, and 1. Interference gives rise to a dramatic difference between the independent emission ($\chi = 0$) and coherent emission ($\chi = 1$) cases. Note that, as indicated above, the distribution for $\chi = 0.02$ for our canonical 140 GeV top will be very different from the expected coherent emission case, and a heavier top with a larger width would lie somewhere in the middle.

We can turn the discussion around to ask under what circumstances we are sensitive to the exact value of Γ . As we have emphasized above and as is clear from Fig. 1, we have maximum sensitivity for χ not too close to 0 or 1. So for $m_t = 140$ GeV distributions of 5 GeV gluons are not very sensitive to a Standard Model Γ , but if we could observe 1 GeV gluons or if the width were much larger than the Standard Model value, χ would be in a more sensitive range. For a heavy top, though, soft gluons are sensitive to the Standard Model width, which follows from the value of χ in the 200 GeV example above.

Now this out-of-plane distribution has clear, simple properties, but it is a differential distribution – a snapshot. Let us consider to what extent the characteristics of

¹The factor of ω in the normalization is chosen so that the only ω dependence is in χ , *cf.* Eq. (2.4).

Fig. 1 are retained in integrated distributions. In Figure 2 we show the distribution of gluon radiation out of the $b\bar{b}$ plane, now integrated over $\pm\pi/8$ in each angular direction and over gluon energies from 5 to 10 GeV. Because we have integrated over ω we now use Γ rather than χ to label the curves. We see in Fig. 2 the same structure as in Fig. 1, and we may draw similar conclusions. We also note that integration over these angles represents $\sim 20\%$ of the gluon events.

4.2.2 “Angular ordering” effects

As is well-known, gluon emission off colourless $q\bar{q}$ pairs exhibits so-called angular ordering behavior (see for example Refs. [14,15] and the discussion above in Section 2): If we split the radiation into pieces associated with the quark or the antiquark, then integrate over the azimuthal angle about, say, the quark’s direction of motion, the quark piece of the radiation vanishes for polar angles greater than the $q\text{--}\bar{q}$ angle. (In particular this implies that *all* radiation is suppressed for collinear q and \bar{q} .) This suppression is due to interference between gluons radiated by the q and the \bar{q} . A derivation of this result is given in Appendix E.

Because the width controls the interference in the case of top, we expect to see angular ordering behavior (or not) according to the size of Γ . To explore angular ordering for radiation off b ’s from top decay, we will examine the gluon emission probability integrated over the azimuthal angle ϕ with respect to the b direction for fixed values of θ_{12} . The results for $\theta_{12} = 5^\circ, 30^\circ, 90^\circ$ and 150° are shown in Figures 3(a), 3(b), 3(c), and 3(d), respectively.

Before considering width effects, let us discuss the general features of these curves; for this purpose Fig. 3(c) is the most instructive. The distribution is shown as a function of θ , the gluon’s polar angle with respect to the b direction. First we see, near $\theta = 0$, the dead cone characteristic of emission off heavy quarks: emission is suppressed along the b direction but peaks nearby at the ‘dead-cone’ angle, $\theta_c \sim m_b/E_b \approx 6^\circ$ for $m_t = 140$ GeV. There is something like a dead cone at $\theta = \theta_{12} = 90^\circ$, due to the \bar{b} . The reason for the asymmetry between the b and \bar{b} is that we have integrated about the b azimuthal angle, but we did not separate out the \bar{b} radiation. A final general feature we note is that most of the radiation is in the vicinity of the quarks, so the distribution falls off at very large θ_{12} .

Now we examine how the width affects angular ordering. In Fig. 3(a), $\theta_{12} = 5^\circ$. The azimuthally integrated distribution is shown for $\chi = 0$ (solid line), 0.5 (dotted line), and 1 (dashed line). With the b and \bar{b} so close together, there are not two distinguishable dead cones but one broadened peak. As χ increases from 0 we see suppression of the radiation by the interference, and for $\chi = 1$ the emission is nearly eliminated; recall that for collinear q and \bar{q} we expect no radiation at all. As large as this effect is, however, it is of academic interest only: because b jets have a finite angular spread we can never hope to identify events with this configuration.

In Fig. 3(b) we consider a larger $b\bar{b}$ angular separation, $\theta_{12} = 30^\circ$; we can just begin to discern the effect of the \bar{b} dead cone. We see again that as χ increases from 0 and the interference turns on, emission at angles larger than θ_{12} is suppressed. We get maximum suppression — as much as an order of magnitude — for the coherent case, $\chi = 1$. Between the b and \bar{b} , that is, for $\theta < \theta_{12}$, the width makes no visible difference, but at larger angles the interference is destructive.

In Figure 3(c) we show the same distribution for $\theta_{12} = 90^\circ$. The effect appears less dramatic: for any given θ_1 the difference between $\chi = 0$ and $\chi = 1$ is not very large. However, on closer inspection we notice that the curves cross at $\theta = \theta_{12}$. The radiation outside the b and \bar{b} (*i.e.* $\theta > \theta_{12}$) is again suppressed, but now the radiation between the b and \bar{b} is enhanced, so that the suppression of radiation outside the $b\bar{b}$ pair *relative* to the radiation between is larger than it appears at first. The net interference for this larger θ_{12} is constructive.

We consider a nearly back-to-back $b\bar{b}$ pair in Fig. 3(d) where $\theta_{12} = 150^\circ$. For such a large angular separation there is little room outside the $b\bar{b}$ pair and the entire angular ordering effect amounts to an enhancement of radiation between the b and \bar{b} . This is the well-known ‘string’ [18] or ‘drag’ [19] effect.

As an aside, we recall that all of the effects we discuss are also relevant to photon radiation in the W^+W^- case. A more complete numerical treatment of this will be given elsewhere [13], but in the meantime we give an angular ordering example for illustration. We show in Figure 4 the W^+W^- analogues of Figs. 3(b) and (d), for $\chi = 0$ (solid lines) and 1 (dashed lines). It should be noted that we have not included the effects of initial state radiation, so that this figure corresponds, *e.g.*, to $\gamma\gamma \rightarrow W^+W^-$ rather than to $e^+e^- \rightarrow W^+W^-$. Now because the lepton is nearly massless, the radiation peaks are much sharper than for the b ’s, but otherwise we see similar features: suppression outside and enhancement between the l^- and l^+ for θ_{12} large and small, respectively. However, there is one other important difference: because of the large W width (2 GeV) and lower accessible photon energies, the relevant values of χ reach the width-sensitive range. Furthermore, leptons do not hadronize, so small lepton-antilepton angles are accessible. Given sufficient event numbers, these effects should be observable.

Returning to top, we have seen in Fig. 3, then, that the overall effect of the width on these azimuthally integrated distributions is enhancement between the b and \bar{b} and suppression outside them. This suggests another way to get at the width dependence experimentally: look at the net radiation between and/or outside the $b\bar{b}$ pair. We show in Figures 5(a) and 5(b) distributions integrated over ϕ as in Fig. 3, over gluon energies (again from 5 to 10 GeV) and also over θ . In Fig. 5(a) we integrate θ from 0 to θ_{12} — for the radiation between the b and \bar{b} — and in Fig. 5(b) from θ_{12} to π — for the radiation outside.

In Fig. 5(a) we see the enhancement of radiation between the b and \bar{b} as the width increases, and, as suggested in Fig. 3, the effect increases with increasing θ_{12} . The

radiation outside the $b\bar{b}$ pair shown in Fig. 5(b) exhibits suppression of emission as the width increases. The largest effect here is at small θ_{12} ; however we cannot hope to do a measurement at very small angular separations because, again, b jets have finite angular size. In both of these figures we see, as we did in Fig. 2, that the Standard Model width for $m_t = 140$ GeV, 0.7 GeV (dotted line) gives distributions very close to those for independent emission, and that sensitivity to Γ is only obtained in the few GeV range.

4.2.3 Integrated distribution

Finally we integrate over all angles and gluon energies from 5 to 10 GeV to show the total soft gluon emission probability as a function of θ_{12} in Figure 6. As we shall see below when we discuss event rates, this may be the only distribution we have very much hope of seeing without multi-decades of collider runs. The independent emission case, $\Gamma = 0$, is, as always, completely independent of θ_{12} due to the absence of interference. Increasing the width turns on the interference and induces θ_{12} dependence. The interference is destructive at small θ_{12} and constructive at large θ_{12} , and we see the crossover point $\Theta_{\text{crit}} \approx 75^\circ$ discussed in Appendix B. Also evident here is the complete suppression of all radiation for the coherent case (large Γ) when the b and \bar{b} are collinear. And, again, there is sensitivity to Γ as it approaches the few GeV range, *i.e.* as it becomes comparable to the gluon energies we consider. Finally, note that the gluon emission probabilities are of the order of 20%.

4.3 Event rates

This brings us to a discussion of event rates and the prospects for measuring the top width from soft gluon distributions. We must re-emphasize that our results are at the parton level, and any realistic assessment must incorporate hadronization of the b 's and gluons as well as detector resolutions and acceptances, etc. Having said that, we now look at cross sections. The cross section for $t\bar{t}$ production near threshold for $m_t = 140$ GeV is about 1 pb [21]. If we assume a yearly luminosity of 10 fb^{-1} , this implies 10^4 $t\bar{t}$ events per year. We saw in the previous subsection that the number of events with a soft gluon is roughly 20% of the lowest order rate, or 2000 events. If we further require leptonically (e or μ) decaying W 's, we are reduced to about 100 events/year. This is less than promising, but not quite hopeless. If there is no other viable way to measure the top width, soft gluon distributions may be an option.

5 Conclusions

How well does measuring the top width from soft gluon radiation in $e^+e^- \rightarrow t\bar{t}$ compare with the standard technique of scanning the threshold structure of the total cross

section? Each method has its disadvantages. The threshold structure is subject to uncertainties from beamstrahlung and beam energy spread, and from theoretical higher order corrections and dependence on parameters like m_t and α_s . The soft gluon radiation method avoids these problems, but it is a higher order process with a lower event rate. The two methods could therefore be considered as complementary – the threshold cross section loses sensitivity with increasing width, but as we have seen, the gluon radiation pattern becomes *more* sensitive at larger Γ for accessible gluon energies. For most of the expected top mass range, the threshold structure method *is* probably better, but if m_t and Γ are large, then examining soft gluons may be more useful.

In summary, we have seen that the top quark’s large width gives rise to new effects from the interplay between the strong and weak interactions, and that the top width affects the distributions of soft gluons radiated in top events. Near the $t\bar{t}$ threshold, the effect of the width is to suppress the *interference* between gluons radiated by the b and \bar{b} , in contrast to the expectation of coherent radiation from the $b\bar{b}$ pair. The sensitivity of the gluon distribution to Γ is largest for gluons with energy $\omega \sim \Gamma$. If 5 GeV corresponds to a realistic minimum energy for measurable gluon jets, then the Standard Model width of a 140 GeV top quark is sufficiently smaller than this to almost completely suppress the interference.

Note that the results of our analysis could in principle be incorporated into a Monte Carlo scheme for generating final states in $e^+e^- \rightarrow t\bar{t} \rightarrow W^+bW^-\bar{b}$ events. Contrary to the standard expectation (see for example [22]), the $b\bar{b}$ antenna is practically inactive here since the bulk of the radiation, that is primary gluons with $\omega > \Gamma$ (in the top rest frame), is governed by the $t\bar{b}$ and $\bar{t}b$ antennae, and is thus unaffected by the relative $b\bar{b}$ orientation angle $\theta_{b\bar{b}}$. When parton cascades are included in the picture, the corresponding hard scale Q is given by

$$Q \sim E_b \approx \frac{M^2 - M_W^2}{2M}. \quad (5.26)$$

The only particles which *are* sensitive to $\theta_{b\bar{b}}$ are those originating from primary bremsstrahlung gluons with $\omega \lesssim \Gamma$, whose yield is determined by the parton cascade scale $Q \sim \Gamma$.

Finally, we have also extended our analysis to the case of photon radiation near threshold in $e^+e^- \rightarrow W^+W^-$, including both hadronic and leptonic W decays. This is especially relevant for LEP200, where the measurement of soft photons with $\omega \sim \Gamma_W$ would also reveal interesting interference effects. We will present numerical results for this elsewhere [13].

Acknowledgements

This work was supported in part by the Texas National Research Laboratory Commission and the United Kingdom Science and Engineering Research Council. Yu.L.D.

and L.H.O thank the Center for Particle Theory at the University of Durham for hospitality while some of this work was being completed. We are grateful to D. Borden, V. Gribov, P. Mättig, M. Perl and M. Swartz for useful discussions.

A Semi-classical derivation of the radiation pattern

The decay of a heavy t quark at rest produces a fast-moving b quark and thus causes acceleration of the colour charge. We are interested in gluon bremsstrahlung induced by this acceleration. Analogously to the treatment of classical electromagnetic currents [20], the colour field formation is conveniently described in terms of Lienard-Wiechert potentials. Thus the two quark currents which participate in the colour field formation are:

$$\vec{j}_1 = \vec{v}_1 \delta^3(\vec{r} - \vec{v}_1(t - t_{01})) \cdot \vartheta(t - t_{01}), \quad (\text{A.1a})$$

$$\vec{j}_2 = \vec{v}_2 \delta^3(\vec{r} - \vec{v}_2(t - t_{02})) \cdot \vartheta(t - t_{02}), \quad (\text{A.1b})$$

where t_{i0} are the times of the two decays. The emission amplitude for the field component with the 4-momentum (ω, \vec{k}) is proportional to the Fourier transformed total current, which we write introducing the effective ‘‘colour charge’’ as

$$\vec{j}(k) = \sqrt{g_s^2 C_F} (\vec{j}_1(k) - \vec{j}_2(k)), \quad (\text{A.2})$$

where the relative minus sign reflects the opposite charges, and $g_s^2 = 4\pi\alpha_s$. For each of the two terms of (A.2) we have

$$\begin{aligned} \vec{j}_i(k) &= \int_{-\infty}^{\infty} dt \int d^3r e^{ix^\mu k_\mu} \vec{j}_i(t, \vec{r}) \\ &= \vec{v}_i \frac{i}{k^0 - (\vec{k} \cdot \vec{v}_i)} \cdot e^{ik^0 t_{0i}}. \end{aligned} \quad (\text{A.3})$$

The field potential induced by the current (A.3) at large (positive) time x^0 reads

$$\vec{A}_i(x) = \int \frac{d^4k}{(2\pi)^4} e^{-ix^\mu k_\mu} [-2\pi i \delta(k^2)] \cdot \vec{j}_i(k) = \int \frac{d^3k}{2\omega(2\pi)^3} e^{-i\omega x^0 + i(\vec{k} \cdot \vec{x})} \cdot \vec{A}_i(k). \quad (\text{A.4})$$

The momentum Fourier component of the total vector field is given by

$$\vec{A}(k) = \sqrt{g_s^2 C_F} (\vec{A}_1(k) - \vec{A}_2(k)); \quad (\text{A.5a})$$

$$\vec{A}_i(k) = \frac{\vec{v}_i}{\omega(1 - v_i \cos \theta_i)} \cdot e^{i\omega t_{0i}}; \quad \omega = |\vec{k}|, \quad (\vec{k} \cdot \vec{v}_i) = \omega v_i \cos \theta_i. \quad (\text{A.5b})$$

To calculate the radiation probability we square the projections of the full field amplitude (A.5a) onto two ‘‘physical’’ gluon states \vec{e}_λ , where $(\vec{e}_\lambda \cdot \vec{k}) = 0$, $(\vec{e}_\lambda)^2 = 1$, and sum over polarizations to obtain

$$dN = \frac{d^3k}{2\omega(2\pi)^3} \sum_{\lambda=1,2} |\vec{A}(k) \cdot \vec{e}_\lambda|^2 = \frac{d^3k}{2\omega(2\pi)^3} \sum_{\alpha,\beta=1,2,3} A^\alpha(k) \cdot \left[\delta_{\alpha\beta} - \frac{k_\alpha k_\beta}{\vec{k}^2} \right] \cdot A^{*\beta}(k). \quad (\text{A.6})$$

Substituting for the vector field from (A.5) and making use of the relations

$$v_{i\alpha} \left[\delta_{\alpha\beta} - \frac{k_\alpha k_\beta}{\vec{k}^2} \right] v_{i\beta} = v_i^2 \sin^2 \theta_i, \quad (\text{A.7a})$$

$$v_{1\alpha} \left[\delta_{\alpha\beta} - \frac{k_\alpha k_\beta}{\vec{k}^2} \right] v_{2\beta} = v_1 v_2 (\cos \theta_{12} - \cos \theta_1 \cos \theta_2), \quad (\text{A.7b})$$

we conclude that the $|A_1|^2$ and $|A_2|^2$ terms reproduce the sum of the “independent” radiation contributions $\mathcal{R}_{\text{indep.}}$ (2.1) while the interference $2 \text{Re}(A_1 A_2^*)$ is proportional to $2\mathcal{J}$ (2.2). So finally we arrive at

$$dN = \frac{d\omega}{\omega} \frac{d\Omega}{4\pi} \frac{C_F \alpha_s}{\pi} \cdot \left\{ \mathcal{R}_1 + \mathcal{R}_2 + 2 \text{Re} e^{i\omega(t_{01}-t_{02})} \cdot \mathcal{J} \right\}. \quad (\text{A.8})$$

This expression describes the radiation accompanying the process with heavy top quarks decaying at times t_{0i} after the $t\bar{t}$ production. These times are not measured, but are distributed according to the decay exponentials

$$\left[\Gamma \int_0^\infty dt_0 e^{-\Gamma t_0} \right]. \quad (\text{A.9})$$

Substituting (A.8) into the decay-time integrals we see that the interference term gives the χ factor,

$$\langle e^{\pm i\omega t_{0i}} \rangle_i \equiv \Gamma \int_0^\infty dt_{0i} e^{-\Gamma t_{0i}} \cdot e^{\pm i\omega t_{0i}} = \frac{\Gamma}{\Gamma \mp i\omega}, \quad (\text{A.10a})$$

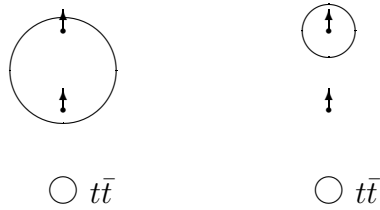
$$\langle \langle e^{\pm i\omega(t_{01}-t_{02})} \rangle_1 \rangle_2 = \frac{\Gamma}{\Gamma + i\omega} \frac{\Gamma}{\Gamma - i\omega} = \chi(\omega), \quad (\text{A.10b})$$

leading to the final expression which is identical to the representation (2.5).

Thus we conclude that the ω -dependence of the soft radiation is due to incoherence induced by the uncertainty $\Delta t_0 \sim \Gamma^{-1}$ in the acceleration times of the two (b -quark) charges. Such a delay can be resolved by a gluon with a *small* wavelength

$$\lambda \sim \omega^{-1} \lesssim \langle \Delta t_0 \rangle \sim \Gamma^{-1}$$

in which case ($\omega \gtrsim \Gamma$) the coherence gets lost and the radiation pattern reduces to the sum of the two independent b and \bar{b} contributions, *i.e.* $\hat{t}\bar{b}$ and $\widehat{\bar{t}}b$ antennas, (see (2.7a)). On the other hand, for wavelengths *large* compared to Γ^{-1} , the (2.7b) regime, the time delay does not affect the radiation: coherence remains undisturbed and the pattern is given by the $b\bar{b}$ antenna describing the point-like production of the “light” quark pair, just as if there was no $t\bar{t}$ stage at all. The two situations can be represented pictorially as shown below.



Note that the result (A.10b) for the decay profile function can easily be generalized to the case of *different* decay widths. This arises, for example, in the case of the production and decay of a pair of different supersymmetric particles, for example $\tilde{q}\tilde{g}$, where the decay width of the decaying particles could in principle be very different. In the general case we obtain

$$\chi(\omega) = \text{Re} \left\{ \frac{\Gamma_1}{\Gamma_1 + i\omega} \frac{\Gamma_2}{\Gamma_2 - i\omega} \right\} = \frac{\Gamma_1 \Gamma_2 (\Gamma_1 \Gamma_2 + \omega^2)}{(\Gamma_1^2 + \omega^2)(\Gamma_2^2 + \omega^2)}. \quad (\text{A.11})$$

For example, for very different decay times, say $\Gamma_1 \gg \Gamma_2$ (and $\omega \sim \Gamma_2$) the expression (A.11) would lead us back to the original

$$\chi(\omega) = \frac{\Gamma_2^2}{\Gamma_2^2 + \omega^2}.$$

However we note, in this context, that our perturbative treatment of gluon emission only makes sense if $\omega > \mu \sim 1 \text{ fm}^{-1}$. Unfortunately this means we cannot discuss in this way the interesting cases of charged Higgs decay $H^+ \rightarrow t\bar{b}$ or single top production $gW^+ \rightarrow t\bar{b}$ where $\Gamma_b \ll \mu$ and $\chi \ll 1$.

B Angular-integrated distributions in $e^+e^- \rightarrow t\bar{t}$

Using the result

$$\int_{-1}^1 d\cos\theta \frac{v^2 \sin^2\theta}{(1-v\cos\theta)^2} = \frac{2}{v} \ln \frac{1+v}{1-v} - 4, \quad (\text{B.1})$$

we see that the angular-integrated contributions of the independent terms are

$$\int \frac{d\Omega}{4\pi} \mathcal{R}_{\text{indep.}} = \frac{1}{v_i} \ln \frac{1+v_i}{1-v_i} - 2 \equiv \mathcal{I}(v_i), \quad (i=1,2). \quad (\text{B.2})$$

The coherent contribution (2.2) contains the integral

$$\int \frac{d\Omega}{4\pi} \frac{2(1-v_1v_2\cos\theta_{12})}{(1-v_1\cos\theta_1)(1-v_2\cos\theta_2)} = \int \frac{d\Omega}{2\pi} \frac{\omega^2 (p_1p_2)}{(p_1k)(p_2k)} = \frac{1}{r} \ln \frac{1+r}{1-r}; \quad (\text{B.3})$$

where

$$r \equiv \sqrt{1 - \frac{(1-v_1^2)(1-v_2^2)}{(1-v_1v_2\cos\theta_{12})^2}} = \sqrt{1 - \frac{M_1^2 M_2^2}{(p_1p_2)^2}}, \quad (\text{B.4})$$

the Lorentz-invariant quantity that is closely related to the relative quark velocity in the rest frame of the pair. In terms of the invariant energy $s = (p_1 + p_2)^2$ and the c.m.s. momentum

$$p_c^2 = \frac{[s - (M_1 + M_2)^2][s - (M_1 - M_2)^2]}{4s} \quad (\text{B.5})$$

one has

$$r = \frac{2p_c \sqrt{s}}{s - (M_1^2 + M_2^2)}. \quad (\text{B.6})$$

For the case of equal masses, $M_1 = M_2$, (B.4) is related to the quark c.m.s. velocity v_c by

$$r = \frac{2v_c}{1+v_c^2}. \quad (\text{B.7})$$

Combining (B.3) with the two remaining terms of (2.2) which give a constant subtraction, we obtain (*cf.* (B.2))

$$\int \frac{d\Omega}{4\pi} \mathcal{R}_{\text{coher.}} = \frac{1}{r} \ln \frac{1+r}{1-r} - 2 = \mathcal{I}(r). \quad (\text{B.8})$$

Putting everything together gives, for the angular integrated radiation yield,

$$\begin{aligned} \frac{dN}{d\omega} &= \frac{C_F \alpha_s}{\pi \omega} \left\{ (1 - \chi(\omega)) \left[\frac{1}{v_1} \log \frac{1+v_1}{1-v_1} + \frac{1}{v_2} \log \frac{1+v_2}{1-v_2} - 4 \right] \right. \\ &\quad \left. + \chi(\omega) \left[\frac{1}{r} \log \frac{1+r}{1-r} - 2 \right] \right\}. \end{aligned} \quad (\text{B.9})$$

We see that the total radiation splits into incoherent and coherent contributions,

$$\frac{dN}{d\omega} = \frac{C_F \alpha_s}{\pi \omega} \{ (1 - \chi(\omega)) \cdot [\mathcal{I}(v_1) + \mathcal{I}(v_2)] + \chi(\omega) \cdot \mathcal{I}(r) \} , \quad (\text{B.10})$$

the relative weight of which is controlled by the profile function χ which depends on the ω/Γ ratio. The first contribution consists of two $\mathcal{I}(v_i)$ terms describing independent radiation off quark antennae “attached” to the c.m.s. (*i.e.* in the rest frame of the decaying top quarks). The function \mathcal{I} can be expressed in terms of the “4-angle” η of the quark momentum as

$$\mathcal{I}(v_i) = 2 \left(\frac{\eta_i}{\tanh(\eta_i)} - 1 \right) ; \quad v_i = \tanh(\eta_i) . \quad (\text{B.11})$$

The coherent contribution, in contrast, carries no information about the initial $t\bar{t}$ system but depends exclusively on the relative motion of the two final colour charges, the (12) antenna. The argument of the corresponding \mathcal{I} factor here is the relative “4-angle” between the quarks,

$$\mathcal{I}(r) = 2 \left(\frac{\Delta}{\tanh(\Delta)} - 1 \right) ; \quad r = \tanh(\Delta) , \quad (\text{B.12})$$

where $\Delta = \eta_1 + \eta_2$ has to be calculated in a reference frame where $q\bar{q}$ are *anti-collinear* (*e.g.* in the c.m.s. of the pair).

In practice, we are usually working in the ultra-relativistic limit $(1 - v_i) \ll 1$, where Eq. (B.9) is dominated by the logarithmic collinear singularities. Since the angular integral of the interference term \mathcal{J} (Eq. (2.2)) converges at $v_1 = v_2 = 1$, one would expect the main collinear contributions $\propto \log(1 - v_i)$ to be ω -independent. To verify this let us keep only the non-vanishing logarithmic and constant terms in (B.9), neglecting powers of $(1 - v_i) \ll 1$. We can approximate (B.4) as

$$r^2 \approx 1 - \frac{4(1 - v_1)(1 - v_2)}{[1 - \cos \theta_{12} + [(1 - v_1) + (1 - v_2)] \cos \theta_{12}]^2} . \quad (\text{B.13})$$

Thus for θ_{12} values not particularly close to 0, so that we can neglect the second term in the denominator compared to the first, we obtain

$$1 - r \approx 2 \cdot \frac{(1 - v_1)(1 - v_2)}{(1 - \cos \theta_{12})^2} \ll 1 , \quad (\text{B.14})$$

and the expression in curly brackets in (B.9) becomes

$$\{ \} \approx \left[\ln \frac{2}{1 - v_1} + \ln \frac{2}{1 - v_2} - 4 \right] + 2\chi(\omega) \left[\ln \frac{1 - \cos \theta_{12}}{2} + 1 \right] . \quad (\text{B.15})$$

Thus we have verified that the main “collinear” contributions are ω -independent in the region of relative quark angles θ_{12} *exceeding* the aperture of the corresponding “dead cones”. It is interesting to compare the relative size of the two terms in (B.15) in practice. For example, for the case of a 140 GeV top quark pair we find

$$\{ \} \simeq 7.9 + 2\chi(\omega) \left[\ln \frac{1 - \cos \theta_{12}}{2} + 1 \right],$$

showing that the integrated quantity is indeed quite sensitive to χ and hence to the width. (In contrast, for a WW pair decaying to muons and neutrinos the numerical term from the logarithms is 23, and the sensitivity to Γ is much decreased.) One could imagine, for example, measuring the profile function χ by studying the θ_{12} variation of the total radiation yield.

Note in particular that the second ω -dependent term in (B.15) *enhances* the radiation at large θ_{12} and acts *destructively* when θ_{12} is chosen below the value Θ_{crit} given by

$$\begin{aligned} \cos \Theta_{\text{crit}} &= 1 - 2 \exp(-1) = 0.26424, \\ \Theta_{\text{crit}} &\approx 75^\circ. \end{aligned} \tag{B.16}$$

It is interesting to notice that the suppression at $\theta_{12} \rightarrow 0$ can be strong enough to completely compensate the main collinear contributions. Indeed, taking parametrically small angles

$$\theta_{12}^2 \ll (1 - v_1) + (1 - v_2),$$

we would obtain for r the value (see (B.13))

$$r^2 \approx \frac{(v_1 - v_2)^2}{[(1 - v_1) + (1 - v_2)]^2} \tag{B.17}$$

which can be arbitrarily small for nearly equal quark velocities. If $r \ll 1$ the second (coherent) term in the general expression (B.9) for the radiation yield becomes negligible and one is left with ($v \equiv v_1 \approx v_2$)

$$\frac{dN}{d\omega} \approx 2 \frac{C_F \alpha_s}{\pi \omega} \cdot (1 - \chi(\omega)) \left[\frac{1}{v} \ln \frac{2}{1 - v} - 2 \right].$$

The result vanishes when $\chi(\omega) \rightarrow 1$ (*i.e.* for $\omega \ll \Gamma$). This corresponds to the total coherent suppression of radiation off two opposite charges moving in the same direction with equal velocities. Notice that for $\omega = \Gamma$ the independent radiation off collinear daughter particles is suppressed by a factor 2.

It is worth mentioning that the ω -dependent coherent effect cancels after integration over all angles θ_{12} . This means that the interference \mathcal{J} does not affect the

total bremsstrahlung caused by the decay of the heavy unstable objects, but only redistributes the accompanying radiation between configurations with different relative angles θ_{12} . This can be checked explicitly by evaluating the angular integral of the second (coherent) term of (B.9) over θ_{12} which results in

$$\begin{aligned} \int_0^\pi \sin \theta_{12} d\theta_{12} \int \frac{d\Omega}{4\pi} \mathcal{R}_{\text{coher.}} &= \int_{-1}^{+1} d \cos \theta_{12} \left[\frac{1}{r} \ln \frac{1+r}{1-r} - 2 \right] \\ &= 2 \cdot \left\{ \frac{1}{v_1} \ln \frac{1+v_1}{1-v_1} + \frac{1}{v_2} \ln \frac{1+v_2}{1-v_2} - 4 \right\} \equiv \int_0^\pi \sin \theta_{12} d\theta_{12} \cdot \int \frac{d\Omega}{4\pi} \mathcal{R}_{\text{indep.}} . \end{aligned} \quad (\text{B.18})$$

This suggests a way of extracting the profile function $\chi(\omega)$ by studying the coherent “redistribution” effects in the total radiation yield. This could be done for example by comparing the gluon yield at fixed θ_{12} below and above the Θ_{crit} value.

Let us consider, therefore, the integrated quantity characterising the interference effects, namely the difference of the integrals over the $b\bar{b}$ opening angles *above* and *below* Θ_{crit} :

$$\delta \equiv \frac{1}{(1 + \cos \Theta_{\text{crit}})} \int_{\Theta_{\text{crit}}}^\pi \sin \theta_{12} d\theta_{12} \frac{\omega dN}{d\omega} - \frac{1}{(1 - \cos \Theta_{\text{crit}})} \int_0^{\Theta_{\text{crit}}} \sin \theta_{12} d\theta_{12} \frac{\omega dN}{d\omega}. \quad (\text{B.19})$$

The normalization in (B.19) is chosen so that the θ_{12} -*independent* contributions cancel. Within the relativistic approximation, we have for (B.15)

$$\mathcal{N} = \mathcal{R}_{\text{indep.}} + 2\chi(\omega) \cdot \left[\ln \frac{1 - \cos \theta_{12}}{2} + 1 \right]. \quad (\text{B.20})$$

Making use of the definition of the critical angle (B.16), we calculate the integrals

$$\frac{1}{(1 + \cos \Theta_{\text{crit}})} \int_{-1}^{\cos \Theta_{\text{crit}}} d \cos \theta_{12} \left[\ln \frac{1 - \cos \theta_{12}}{2} + 1 \right] = \frac{1 - \cos \Theta_{\text{crit}}}{1 + \cos \Theta_{\text{crit}}}, \quad (\text{B.21a})$$

$$\frac{1}{(1 - \cos \Theta_{\text{crit}})} \int_{\cos \Theta_{\text{crit}}}^1 d \cos \theta_{12} \left[\ln \frac{1 - \cos \theta_{12}}{2} + 1 \right] = -1; \quad (\text{B.21b})$$

to obtain finally for (B.19)

$$\delta = \frac{C_F \alpha_s}{\pi} \frac{4}{1 + \cos \Theta_{\text{crit}}} \cdot \chi(\omega). \quad (\text{B.22})$$

Invoking the numerical value of the critical angle (B.16) we write (B.22) as

$$\delta = 4.218 \frac{\alpha_s(\omega)}{\pi} \cdot \chi(\omega). \quad (\text{B.23})$$

Notice that we have chosen here the gluon energy as the argument of the running coupling, since it is *large* gluon energies that contribute to (B.23).

C Initial and final state radiation in $e^+e^- \rightarrow W^+W^-$ near threshold

Let us denote by \vec{v}_0 ($-\vec{v}_0$) the 3-velocities of the incoming e^+ (e^-). Then the initial state electromagnetic current takes the form

$$\vec{j}_0 = \left[\vec{v}_0 \delta^3(\vec{r} - \vec{v}_0 t) - (-\vec{v}_0) \delta^3(\vec{r} + \vec{v}_0 t) \right] \cdot \vartheta(-t) \quad (\text{C.1})$$

which gives an extra contribution to the field amplitude (see Appendix A)

$$\vec{A}_0 = -\frac{\vec{v}_0}{\omega} \left[\frac{1}{1 - (\vec{v}_0 \vec{n})} + \frac{1}{1 + (\vec{v}_0 \vec{n})} \right] = -\frac{\vec{v}_0}{\omega} \frac{2}{1 - v_0^2 \cos^2 \theta_0}, \quad (\text{C.2})$$

where \vec{n} is direction of the photon and θ_0 its angle with respect to the incoming *positron*. Since the e^+e^- “disappear” at the same time as the WW pair is produced, the amplitude (C.2) is real with our convention ($t=0$). Let us choose for the sake of simplicity the $(\ell\nu\ell\nu)$ decay channel of the WW . We use (A.6) to obtain for the radiation probability

$$\begin{aligned} dN &= e^2 \frac{d^3k}{2\omega(2\pi)^3} \sum_{\lambda=1,2} \left| \vec{A}(k) \cdot \vec{e}_\lambda \right|^2 = \frac{e^2}{4\pi^2} \frac{d\omega}{\omega} \frac{d\Omega_{\vec{n}}}{4\pi} \sum_{\alpha,\beta=1,3} a^\alpha(k) [\delta_{\alpha\beta} - n_\alpha n_\beta] a^{*\beta}(k), \\ \vec{a}(k) &= \frac{\vec{v}_1}{1 - (\vec{v}_1 \vec{n})} \cdot e^{i\omega t_{01}} - \frac{\vec{v}_2}{1 - (\vec{v}_2 \vec{n})} \cdot e^{i\omega t_{02}} - \frac{2\vec{v}_0}{1 - (\vec{v}_0 \vec{n})^2}, \end{aligned} \quad (\text{C.3})$$

where \vec{v}_1, \vec{v}_2 stand for positively and negatively charged final state leptons respectively. The novel feature of (C.3) is an interference between the initial state radiation (ISR) (the last term) and the final state radiation (FSR) (the first two terms), which has the structure

$$\mathcal{J}_{01} \cdot 2 \operatorname{Re} e^{i\omega t_{01}} + \mathcal{J}_{02} \cdot 2 \operatorname{Re} e^{i\omega t_{02}}. \quad (\text{C.4})$$

After the integration over the W^\pm decay times t_{0i} is performed (see (A.10)) it gives rise to the same profile function χ , due to the identity

$$\operatorname{Re} \left\{ \frac{\Gamma}{\Gamma + i\omega} \frac{\Gamma}{\Gamma - i\omega} \right\} = \operatorname{Re} \left\{ \frac{\Gamma}{\Gamma \pm i\omega} \right\} = \frac{\Gamma^2}{\Gamma^2 + \omega^2} \equiv \chi(\omega). \quad (\text{C.5})$$

The final answer can therefore be represented as

$$dN = \frac{\alpha}{\pi} \frac{d\omega}{\omega} \frac{d\Omega_{\vec{n}}}{4\pi} [\mathcal{N}_{\text{FS}} + \mathcal{N}_{\text{IS}} + \mathcal{N}_{\text{I/F}}] \quad (\text{C.6})$$

where the first term is, as before (*cf.* (2.5)),

$$\mathcal{N}_{\text{FS}} = \mathcal{R}_1 + \mathcal{R}_2 + 2\chi(\omega) \cdot \frac{(\vec{v}_1 \vec{n})(\vec{v}_2 \vec{n}) - (\vec{v}_1 \vec{v}_2)}{[1 - (\vec{v}_1 \vec{n})][1 - (\vec{v}_2 \vec{n})]}. \quad (\text{C.7a})$$

The new terms describe independent radiation off the initial state e^+e^- antenna,

$$\mathcal{N}_{\text{IS}} = \frac{4v_0^2 \sin^2 \theta_0}{(1 - v_0^2 \cos^2 \theta_0)^2}, \quad (\text{C.7b})$$

and the ISR/FSR interference contribution

$$\mathcal{N}_{\text{I/F}} = 2\chi(\omega) \cdot \frac{2}{1 - (\vec{v}_0 \vec{n})^2} \left\{ \frac{(\vec{v}_0 \vec{n}) - (\vec{v}_0 \vec{v}_1)}{1 - (\vec{v}_1 \vec{n})} - \frac{(\vec{v}_0 \vec{n}) - (\vec{v}_0 \vec{v}_2)}{1 - (\vec{v}_2 \vec{n})} \right\}. \quad (\text{C.7c})$$

Note that the ISR/FSR interference (C.7c) vanishes (i) after integration over the angles between the ISR and FSR antennae (keeping the relative angle between the daughter charged particles fixed), and (ii) in the limit $\omega \gg \Gamma$, as expected. We recall also that both \mathcal{N}_{IS} and $\mathcal{N}_{\text{I/F}}$ vanish when the kinematic limit $\omega > \omega_{max}^{\text{IS}}$ (Eq. (3.12)) is exceeded.

In practice we are not interested in photon emission close to the beam direction, and so for $\theta_0 \gg m_e/M_W$ we can set $v_0 = 1$ and the above expressions become

$$\mathcal{N}_{\text{IS}} \simeq \frac{4}{\sin^2 \theta_0}, \quad (\text{C.8})$$

and

$$\mathcal{N}_{\text{I/F}} = \chi(\omega) \cdot \mathcal{N}_{\text{IS}} \cdot \left\{ \frac{\cos \theta_0 - (\vec{v}_0 \vec{v}_1)}{1 - (\vec{v}_1 \vec{n})} - \frac{\cos \theta_0 - (\vec{v}_0 \vec{v}_2)}{1 - (\vec{v}_2 \vec{n})} \right\}. \quad (\text{C.9})$$

D Hadronic W^+W^- decays

In this Appendix we derive the expressions for the photon radiation pattern in $e^+e^- \rightarrow W^+W^-$ when at least one of the W 's decays *hadronically*, *i.e.* to $q\bar{q}'$. Consider first the case when both W 's decay hadronically. The two currents are then (see Eq.(3.16))

$$\begin{aligned} j_1^\mu &= Q \frac{p_1^\mu}{(kp_1)} + (1-Q) \frac{\bar{p}_1^\mu}{(k\bar{p}_1)} - \frac{q^\mu}{(kq)}, \\ j_2^\mu &= Q' \frac{p_2^\mu}{(kp_2)} + (1-Q') \frac{\bar{p}_2^\mu}{(k\bar{p}_2)} - \frac{q^\mu}{(kq)}, \end{aligned} \quad (\text{D.1})$$

where $Q = Q' = \frac{2}{3}$ and p_1, p_2 denote the momenta of the up -type quark and antiquark respectively. In the 3-vector form ($(eq) = 0$) we can write

$$\vec{j} = \frac{\vec{v}}{\omega} \left[\frac{Q}{1 - \vec{n}\vec{v}} - \frac{1-Q}{1 + \vec{n}\vec{v}} \right] = \frac{\vec{v}}{\omega} \frac{(2Q-1) + \vec{n}\vec{v}}{1 - (\vec{n}\vec{v})^2} \quad (\text{D.2})$$

where we have treated the quark and the accompanying antiquark momenta as *anti-parallel* and of equal mass. Then

$$\begin{aligned} \mathcal{N}^{(qq)} &\propto \left[(e\vec{v}_1) \frac{(2Q-1) + \vec{n}\vec{v}_1}{1 - (\vec{n}\vec{v}_1)^2} \right]^2 + \left[(e\vec{v}_2) \frac{(2Q'-1) + \vec{n}\vec{v}_2}{1 - (\vec{n}\vec{v}_2)^2} \right]^2 \\ &\quad - 2\chi(\omega) \cdot (e\vec{v}_1)(e\vec{v}_2) \left[\frac{(2Q-1) + \vec{n}\vec{v}_1}{1 - (\vec{n}\vec{v}_1)^2} \right] \left[\frac{(2Q'-1) + \vec{n}\vec{v}_2}{1 - (\vec{n}\vec{v}_2)^2} \right]. \end{aligned} \quad (\text{D.3})$$

For the mixed one-quark-one-leptonic decay configuration, $Q' = 1$ and we have

$$\begin{aligned} \mathcal{N}^{(q\ell)} &\propto \left[(e\vec{v}_1) \frac{(2Q-1) + \vec{n}\vec{v}_1}{1 - (\vec{n}\vec{v}_1)^2} \right]^2 + \left[(e\vec{v}_2) \frac{1}{1 - \vec{n}\vec{v}_2} \right]^2 \\ &\quad - 2\chi(\omega) \cdot (e\vec{v}_1)(e\vec{v}_2) \left[\frac{(2Q-1) + \vec{n}\vec{v}_1}{1 - (\vec{n}\vec{v}_1)^2} \right] \left[\frac{1}{1 - \vec{n}\vec{v}_2} \right]. \end{aligned} \quad (\text{D.4})$$

Experimentally it seems very difficult (if at all possible) to discriminate between the two jets that originate from, say, $W^+ \rightarrow u + \bar{d}$ decay. Without being able to *separate* quark and antiquark jets (Q from $1-Q$) we have to drop in (D.3,D.4) the *odd* terms in $2Q-1$ ($2Q'-1$). After summing over photon polarizations, Eq. (A.7), we arrive at

$$\begin{aligned} \mathcal{N}^{(qq)} &\propto v_1^2 \sin^2 \theta_1 \frac{(2Q-1)^2 + v_1^2 \cos^2 \theta_1}{(1 - v_1^2 \cos^2 \theta_1)^2} + v_2^2 \sin^2 \theta_2 \frac{(2Q'-1)^2 + v_2^2 \cos^2 \theta_2}{(1 - v_2^2 \cos^2 \theta_2)^2} \\ &\quad + 2\chi(\omega) \cdot v_1 v_2 (\cos \theta_1 \cos \theta_2 - \cos \theta_{12}) \left[\frac{v_1 \cos \theta_1}{1 - v_1^2 \cos^2 \theta_1} \right] \left[\frac{v_2 \cos \theta_2}{1 - v_2^2 \cos^2 \theta_2} \right]; \end{aligned} \quad (\text{D.5a})$$

$$\begin{aligned} \mathcal{N}^{(q\ell)} \propto & v_1^2 \sin^2 \theta_1 \frac{(2Q-1)^2 + v_1^2 \cos^2 \theta_1}{(1 - v_1^2 \cos^2 \theta_1)^2} + \frac{v_2^2 \sin^2 \theta_2}{(1 - v_2 \cos \theta_2)^2} \\ & + 2\chi(\omega) \cdot v_1 v_2 (\cos \theta_1 \cos \theta_2 - \cos \theta_{12}) \left[\frac{v_1 \cos \theta_1}{1 - v_1^2 \cos^2 \theta_1} \right] \left[\frac{1}{1 - v_2 \cos \theta_2} \right]. \end{aligned} \quad (\text{D.5b})$$

Recalling the expressions for \mathcal{R}_1 , \mathcal{R}_2 and \mathcal{J} introduced in Section 2, it is straightforward to cast this result in the form given in Eqs. (3.18,3.19). Note that there is a subtlety in the $\mathcal{N}^{(qq)}$ case concerning the definition of the angles. Whereas for the $t\bar{t}$ case we could unambiguously define, say, θ_1 with respect to the b quark, with two indistinguishable jets from the W we lose this capability. However having made a choice for defining θ_1 , the definition of θ_2 is correlated with that of θ_{12} . The invariance of the $\mathcal{N}^{(qq)}$ distribution under this symmetry is manifest by the dependence on the quadratic terms $\cos^2 \theta_1$, $\cos^2 \theta_2$ and $\cos \theta_1 \cos \theta_2$ only.

As long as the photon direction \vec{n} is kept away from the “dead cones” of the final charges, a simplified version of Eqs. (D.5) can be used in which the velocities are set to 1:

$$\mathcal{N}^{(qq)} = \frac{\frac{1}{9} + \cos^2 \theta_1}{\sin^2 \theta_1} + \frac{\frac{1}{9} + \cos^2 \theta_2}{\sin^2 \theta_2} + 2\chi(\omega) \frac{(\cos \theta_1 \cos \theta_2 - \cos \theta_{12}) \cos \theta_1 \cos \theta_2}{\sin^2 \theta_1 \sin^2 \theta_2}; \quad (\text{D.6a})$$

$$\mathcal{N}^{(q\ell)} = \frac{\frac{1}{9} + \cos^2 \theta_1}{\sin^2 \theta_1} + \frac{\sin^2 \theta_2}{(1 - \cos \theta_2)^2} + 2\chi(\omega) \frac{(\cos \theta_1 \cos \theta_2 - \cos \theta_{12}) \cos \theta_1}{\sin^2 \theta_1 (1 - \cos \theta_2)}. \quad (\text{D.6b})$$

Expressing the relative angle θ_{12} between the final jets (the jet and the lepton) in terms of photon angles with respect to the 1,2 directions, we can write the final expression for the angular pattern of photon radiation as

$$\mathcal{N}^{(qq)} \propto \frac{\frac{1}{9} + \cos^2 \theta_1}{\sin^2 \theta_1} + \frac{\frac{1}{9} + \cos^2 \theta_2}{\sin^2 \theta_2} - 2\chi(\omega) \cot \theta_1 \cot \theta_2 \cdot \cos \phi_{12}, \quad (\text{D.7a})$$

$$\mathcal{N}^{(q\ell)} \propto \frac{\frac{1}{9} + \cos^2 \theta_1}{\sin^2 \theta_1} + \cot^2 \frac{\theta_2}{2} - 2\chi(\omega) \cot \theta_1 \cot \frac{\theta_2}{2} \cdot \cos \phi_{12}, \quad (\text{D.7b})$$

where ϕ_{12} is the azimuthal angle between \vec{v}_1 and \vec{v}_2 projections onto the plane *orthogonal* to the photon direction, \vec{n} .

To study the θ_{12} dependence of the *total* photon yield one has to evaluate the integrals over the gluon radiation angle of the interference terms in (D.5). These integrals are finite at $v_1 = v_2 = 1$ so we can use the relativistic approximation (D.6) for this purpose. A straightforward calculation leads then to identical results for the quark-quark and quark-lepton channels, namely

$$\begin{aligned} & \int \frac{d\Omega}{4\pi} \frac{(\cos \theta_1 \cos \theta_2 - \cos \theta_{12}) \cos \theta_1 \cos \theta_2}{\sin^2 \theta_1 \sin^2 \theta_2} \\ & = \int \frac{d\Omega}{4\pi} \frac{(\cos \theta_1 \cos \theta_2 - \cos \theta_{12}) \cos \theta_1}{\sin^2 \theta_1 (1 - \cos \theta_2)} = \ln \frac{\sin \theta_{12}}{2} + 1. \end{aligned} \quad (\text{D.8})$$

Taken together with the independent contributions, the total photon yield then takes the form given in Eqs. (3.22,3.23).

E Azimuthal angle integrations

In this Appendix we derive the expressions for the radiation pattern in $t\bar{t}$ production when the gluon is integrated over its azimuthal angle ϕ with respect to the direction of the b -quark (*i.e.* the “1” direction).

We first note that the ϕ dependence enters when we substitute

$$\cos \theta_2 = \cos \theta_1 \cos \theta_{12} + \cos \phi \sin \theta_1 \sin \theta_{12} \quad (\text{E.1})$$

into the result for $\mathcal{R}_{\text{coher.}}$ given in Eq. (2.2). Consider first the azimuthal average of the interference term, $\langle \mathcal{J} \rangle$. We need the basic integral ($a \geq |b|$)

$$\int_0^{2\pi} \frac{d\phi}{2\pi} \frac{1}{a + b \cos \phi} = \frac{1}{\sqrt{a^2 - b^2}}. \quad (\text{E.2})$$

where

$$a = 1 - v_2 \cos \theta_1 \cos \theta_{12}, \quad b = -v_2 \sin \theta_1 \sin \theta_{12}. \quad (\text{E.3})$$

This gives

$$V \equiv \left\langle \frac{1}{1 - v_2 \cos \theta_2} \right\rangle = \left[A^2 + \sin^2 \theta_1 (1 - v_2^2) \right]^{-\frac{1}{2}}, \quad (\text{E.4})$$

where

$$A = \cos \theta_1 - v_2 \cos \theta_{12}, \quad (\text{E.5})$$

which then leads to

$$\langle J \rangle = \frac{v_1}{1 - v_1 \cos \theta_1} [V \cdot A - \cos \theta_1]. \quad (\text{E.6})$$

As a function of θ_1 the first term in the bracket is a smooth step-function-like distribution, falling from +1 at $\theta_1 = 0$, through 0 at $\cos \theta_1 = v_2 \cos \theta_{12}$ (*i.e.* when θ_1 coincides with the direction of the other b -quark), to -1 at $\theta_1 = \pi$, see also Ref. [15].

For the azimuthal average of the \mathcal{R}_2 contribution to $\mathcal{R}_{\text{coher.}}$ we can make use of the following:

$$V' \equiv \left\langle \frac{1}{(1 - v_2 \cos \theta_2)^2} \right\rangle = \left(v_2 \frac{\partial}{\partial v_2} + 1 \right) V = (1 - v_2 \cos \theta_1 \cos \theta_{12}) \cdot V^3, \quad (\text{E.7})$$

from which follows

$$\langle \mathcal{R}_2 \rangle = 2V - 1 - (1 - v_2^2) V'. \quad (\text{E.8})$$

Note that in the special case when $\theta_{12} = 0$ we obtain

$$\langle J \rangle = -\frac{v_1 v_2 \sin^2 \theta_1}{(1 - v_1 \cos \theta_1)(1 - v_2 \cos \theta_1)}, \quad (\text{E.9})$$

and

$$\langle \mathcal{R}_{\text{coher.}} \rangle = \frac{(v_1 - v_2)^2 \sin^2 \theta_1}{(1 - v_1 \cos \theta_1)^2 (1 - v_2 \cos \theta_1)^2}. \quad (\text{E.10})$$

Evidently $\langle \mathcal{R}_{\text{coher.}} \rangle$ vanishes when $v_1 = v_2$, because of *complete* destructive interference.

A similar analysis can be performed for the more symmetric case of the azimuthal average around the *bisector* of the “1” and “2” directions. If Θ is the angle between the gluon and the bisector and $\Delta = \frac{1}{2}\theta_{12}$ then a straightforward but tedious calculation gives for the independent contributions

$$\langle \mathcal{R}_i \rangle = 2U_i - 1 - (1 - v_i^2)U'_i, \quad (\text{E.11})$$

and for the coherent contribution

$$\langle \mathcal{R}_{\text{coher.}} \rangle = \frac{2(1 - v_1 v_2 \cos 2\Delta)}{v_1 + v_2 - 2v_1 v_2 \cos \Theta \cos \Delta} [v_1 U_1 + v_2 U_2] - (1 - v_1^2)U'_1 - (1 - v_2^2)U'_2, \quad (\text{E.12})$$

where

$$U_i \equiv \left\langle \frac{1}{1 - v_i \cos \Theta_i} \right\rangle = [(1 - v_i^2) \sin^2 \Delta + (\cos \Delta - v_i \cos \Theta)^2]^{-\frac{1}{2}}, \quad (\text{E.13a})$$

$$U'_i \equiv \left\langle \frac{1}{(1 - v_i \cos \Theta_i)^2} \right\rangle = \left(v_i \frac{\partial}{\partial v_i} + 1 \right) U_i = (1 - v_i \cos \Theta \cos \Delta) U_i^3. \quad (\text{E.13b})$$

It can be further shown that for the equal velocities case ($v_1 = v_2 = v$)

$$\begin{aligned} \langle \mathcal{R}_{\text{coher.}} \rangle &= \frac{2v^2 \sin^2 \Delta}{1 - v \cos \Theta \cos \Delta} [2U^{-1} - \sin^2 \Theta (1 - v^2)] U^3 \\ &\propto \Delta^2, \quad \Delta \rightarrow 0, \end{aligned} \quad (\text{E.14})$$

while for $v_1 \neq v_2$ and $\theta_{12} = 0$ we again arrive at (*cf.* Eq. (E.10))

$$\langle \mathcal{R}_{\text{coher.}} \rangle = \frac{(v_1 - v_2)^2 \sin^2 \Theta}{(1 - v_1 \cos \Theta)^2 (1 - v_2 \cos \Theta)^2}. \quad (\text{E.15})$$

References

- [1] Yu.L. Dokshitzer, V.A. Khoze and S.I. Troyan, University of Lund preprint LU-TP-92-10 (1992).
- [2] V.A. Khoze, L.H. Orr and W.J. Stirling, Nucl. Phys. **B378** (1992) 413.
- [3] CDF collaboration: F. Abe *et al.*, Phys. Rev. **D45** (1992) 3921.
- [4] J.H. Kühn, Acta Phys. Austr. Suppl. **24** (1982) 203.
- [5] I.I. Bigi *et al.*, Phys. Lett. **181B** (1986) 157.
- [6] L.H. Orr and J.L. Rosner, Phys. Lett. **246B** (1990) 221; **248** (1990) 474(E).
- [7] G. Jikia, Phys. Lett. **257B** (1991) 196.
- [8] T. Muta, R. Najima and S. Wakaizumi, Mod. Phys. Lett. **A1** (1986) 203.
- [9] G. Altarelli *et al.* in *Physics at LEP*, eds. J. Ellis and R. Peccei, CERN 86-02, vol.1, p.1 (1986).
E. Longo *et al.* in *ECFA Workshop on LEP200*, eds. A. Böhm and W. Hoogland, CERN 87-08, vol.1, p.85 (1987).
- [10] A. Sommerfeld, “*Atombau und Spektrallinien*”, Bd. 2 (Vieweg, Braunschweig) 1939.
- [11] A.D. Sakharov, JETP **18** (1948) 631.
- [12] UA2 collaboration: J. Alitti *et al.*, Phys. Lett. **276B** (1992) 354.
- [13] Yu.L. Dokshitzer, V.A. Khoze, L.H. Orr and W.J. Stirling, in preparation.
- [14] Yu.L. Dokshitzer, V.A. Khoze, A.H. Mueller, and S.I. Troyan, *Basics of Perturbative QCD*, Editions Frontieres, 1991.
- [15] G. Marchesini and B. R. Webber, Nucl. Phys. **B330** (1990) 261.
- [16] M. Lemoine and M. Veltman, Nucl. Phys. **B164** (1980) 443.
- [17] G. E. Abu Leil, University of Durham preprint DTP/92/84 (1992).
- [18] B. Andersson, G. Gustafson and T. Sjöstrand, Phys. Lett. **94B** (1980) 211.
- [19] Ya.I. Azimov *et al.*, Phys. Lett. **165B** (1985) 147.

- [20] See for example: J. M. Jauch and F. Rohrlich, *The theory of photons and electrons: the relativistic quantum field theory of charged particles with spin one-half*, (1976); A.I. Akhiezer and V.B. Berestetskii, *Quantum electrodynamics*, Interscience (1965).
- [21] See for example the report of the Top Quark Physics working group in the Proceedings of the Workshop on e^+e^- collisions at 500 GeV, ed. P.M. Zerwas, DESY 92-123A, p. 255 (1992).
- [22] K. Fujii, KEK Preprint 92-6 (1992), and references therein.

Figure Captions

- [1] Soft gluon distribution in $e^+e^- \rightarrow t\bar{t} \rightarrow b\bar{b}WW$ near $t\bar{t}$ threshold, for gluons perpendicular to the $b\bar{b}$ plane, for χ as marked. $dN/d\omega d\Omega$ is given by Eqs. (2.4) and (4.24), with $\theta_1 = \theta_2 = 90^\circ$. θ_{12} is the angle between the b and \bar{b} . Here and in all subsequent figures, unless otherwise noted, $v = 0.9944$, which corresponds to $m_t = 140$ GeV for $m_b = 5$ GeV and $m_W = 80$ GeV.

- [2] Distribution of soft gluons radiated out of the $b\bar{b}$ plane, with energy and angular integrations, for Γ as marked. The distribution shown is given by

$$\int dN \equiv 2 \int_{5 \text{ GeV}}^{10 \text{ GeV}} d\omega \int_{3\pi/8}^{5\pi/8} \sin \theta d\theta \int_{3\pi/8}^{5\pi/8} d\phi (dN/d\omega d\Omega),$$

where θ and ϕ are, respectively, the polar and azimuthal angles with respect to the b quark direction; the $b\bar{b}$ pair defines the xz plane. The factor of 2 accounts for radiation on both sides of the plane. $\Gamma = 0.7$ GeV (dotted line) corresponds to a Standard Model top with $m_t = 140$ GeV.

- [3] Angular ordering effects in the soft gluon distribution with azimuthal integration:

$$\int dN \equiv \omega(dN/d\omega d \cos \theta) = \int_0^{2\pi} d\phi \omega(dN/d\omega d\Omega).$$

The angles between the b and \bar{b} are (a) $\theta_{12} = 5^\circ$, (b) $\theta_{12} = 30^\circ$, (c) $\theta_{12} = 90^\circ$, and (d) $\theta_{12} = 120^\circ$. Solid lines: $\chi = 0$; dotted lines: $\chi = 0.5$; dashed lines: $\chi = 1$.

- [4] Analog of Fig. 3 for the W^+W^- case: angular ordering effects in the soft *photon* distribution in $\gamma\gamma \rightarrow W^+W^- \rightarrow l^+l^-\nu\bar{\nu}$, for $\theta_{12} = 30^\circ$ and 150° . $\int dN \equiv \omega(dN/d\omega d \cos \theta)$ as in Fig. 3. Solid lines: $\chi = 0$; dashed lines: $\chi = 1$. (The $\gamma\gamma \rightarrow W^+W^-$ case is equivalent to the $e^+e^- \rightarrow W^+W^-$ case with no initial state radiation.)

- [5] Soft gluon distribution (a) “between” and (b) “outside” the $b\bar{b}$ pair. In (a),

$$\int dN \equiv \int_{5 \text{ GeV}}^{10 \text{ GeV}} d\omega \int_0^{2\pi} d\phi \int_0^{\theta_{12}} \sin \theta d\theta (dN/d\omega d\Omega),$$

and in (b),

$$\int dN \equiv \int_{5 \text{ GeV}}^{10 \text{ GeV}} d\omega \int_0^{2\pi} d\phi \int_{\theta_{12}}^{\pi} \sin \theta d\theta (dN/d\omega d\Omega).$$

Solid lines: $\Gamma = 0, \infty$ (as marked); dotted line: $\Gamma = 0.7$ GeV; dashed line: $\Gamma = 3$ GeV; dot-dashed line: $\Gamma = 5$ GeV.

- [6] Net emission probability for gluons with energies from 5 to 10 GeV:

$$\int dN \equiv \int_{5 \text{ GeV}}^{10 \text{ GeV}} d\omega \int_0^{2\pi} d\phi \int_0^{\pi} \sin \theta d\theta (dN/d\omega d\Omega).$$